Environmental Research Letters

LETTER

Ground-level climate at a peatland wind farm in Scotland is affected by wind turbine operation

Alona Armstrong[1,2], **Ralph R Burton**[3], **Susan E Lee**[3,5], **Stephen Mobbs**[3], **Nicholas Ostle**[2,4], **Victoria Smith**[3], **Susan Waldron**[1] **and Jeanette Whitaker**[4]

[1] School of Geographical and Earth Sciences, University of Glasgow, Glasgow G12 8QQ, UK
[2] Lancaster Environment Centre and Energy Lancaster, Lancaster University, Lancaster, LA1 4YQ, UK
[3] National Centre for Atmospheric Science, School of Earth and Environment, University of Leeds, Leeds, LS2 9JT, UK
[4] Centre for Ecology and Hydrology, Lancaster Environment Centre, Library Avenue, Bailrigg, LA1 4AP, UK
[5] Now at School of Civil Engineering, University of Birmingham, Edgbaston, Birmingham, B15 2TT, UK

E-mail: a.armstrong@lancaster.ac.uk

Keywords: wind energy, carbon cycling, microclimate, atmospheric boundary layer

Supplementary material for this article is available online

OPEN ACCESS

RECEIVED
21 December 2015

REVISED
18 March 2016

ACCEPTED FOR PUBLICATION
23 March 2016

PUBLISHED
22 April 2016

Abstract

The global drive to produce low-carbon energy has resulted in an unprecedented deployment of onshore wind turbines, representing a significant land use change for wind energy generation with uncertain consequences for local climatic conditions and the regulation of ecosystem processes. Here, we present high-resolution data from a wind farm collected during operational and idle periods that shows the wind farm affected several measures of ground-level climate. Specifically, we discovered that operational wind turbines raised air temperature by 0.18 °C and absolute humidity (AH) by 0.03 g m^{-3} during the night, and increased the variability in air, surface and soil temperature throughout the diurnal cycle. Further, the microclimatic influence of turbines on air temperature and AH decreased logarithmically with distance from the nearest turbine. These effects on ground-level microclimate, including soil temperature, have uncertain implications for biogeochemical processes and ecosystem carbon cycling, including soil carbon stocks. Consequently, understanding needs to be improved to determine the overall carbon balance of wind energy.

Introduction

Globally the installed electricity generating capacity of wind turbines has increased from 48 to 370 GW over the last decade (2004–2014) (GWEC 2015) and is predicted to increase more than any other renewable energy source by 2035 (IEA 2012). Deployment of this magnitude will result in wind farms covering 293 333 km^2 by 2035 (Denholm *et al* 2009, IEA 2012). Effects of this land use change on human populations and wildlife, including avian and bat communities, have received some consideration (Knopper and Ollson 2011, Pearce-Higgins *et al* 2012, Lovich and Ennen 2013, Northrup and Wittemyer 2013). However, there is a paucity of data on the effects of wind farms on soil and ground-level climates (Baidya Roy and Traiteur 2010, Rajewski *et al* 2013, Smith *et al* 2013, Rajewski *et al* 2014), limiting our ability to determine effects on biogeochemical processes that regulate plant-soil carbon cycling (Armstrong *et al* 2014). This, in turn, could have implications for the true carbon balance of this renewable energy technology.

Wind farms have been postulated to affect climatic conditions from local to global scale through modification of the vertical distribution of energy and moisture within the atmosphere and exchange between the land surface and atmosphere (Baidya Roy *et al* 2004). Previous studies have modelled the effects of turbines (Baidya Roy *et al* 2004, Keith *et al* 2004, Wang and Prinn 2010, Baidya Roy 2011, Fiedler and Bukovsky 2011, Lu and Porté-Agel 2015), measured air temperature differences upwind and downwind of turbines (Baidya Roy and Traiteur 2010, Rajewski *et al* 2013, Smith *et al* 2013, Rajewski *et al* 2014), and used satellite data to examine temperature effects over

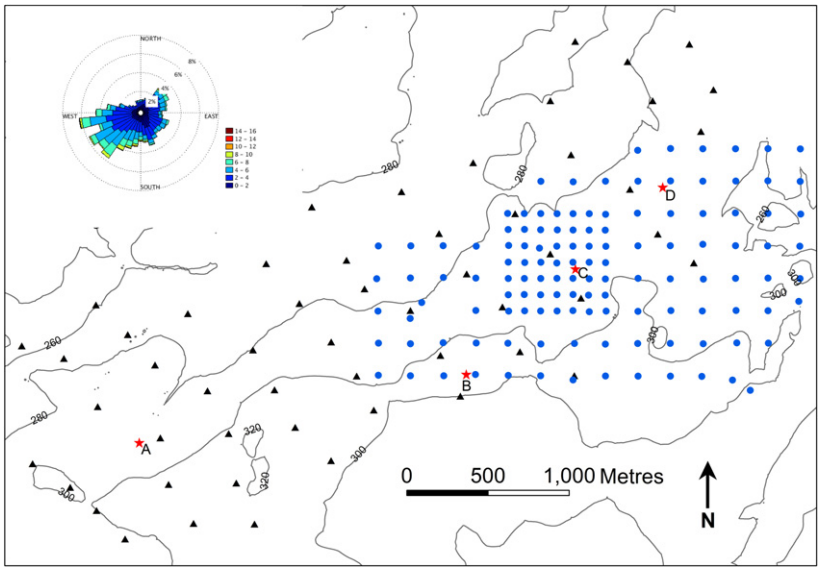

Figure 1. Location of monitoring equipment at Black Law Wind Farm, Scotland (55° 46′ 01″ N 03° 44′ 20″ W). Turbines are denoted by black triangles, the clusters of T_{SU} and T_{SO} sensors denoted by red stars (A–D, 9 sensors at both the surface and subsurface at each location), the T_A and RH sensors by blue circles and the height contours by grey lines. Wind direction was monitored at site B and the inset wind rose depicts wind direction during the study period. The colours denote the wind speeds (m s^{-1}) and the percentage rings indicate the relative frequency of occurrence. Wind directions are plotted according to where the wind originates. Map generated using ArcGIS 10.

a 10 000 km^2 area of North America (Zhou *et al* 2012). More recently, in addition to effects on heat fluxes, one row of turbines was reported to have increased carbon dioxide (CO_2) release from the land during the night and uptake during the day and thus potentially impacting soil carbon stocks (Rajewski *et al* 2014). However, extrapolating results from a single row of turbines is problematic given nonlinear interactions between multiple wakes (Rajewski *et al* 2014). To fully resolve the implications of microclimatic influences on biogeochemical processes in hosting ecosystems, high-resolution spatially explicit field data are needed when turbines are operational and idle. Moreover, these studies need to establish if wind turbine-induced differences are measureable beyond that of natural variation (Rajewski *et al* 2014).

To assess whether there were operational wind turbine-induced changes to the microclimate at a terrestrial wind farm of a magnitude to impact ecosystem carbon processes we measured absolute humidity (AH), and air, surface and soil temperature (T_A, T_{SU} and T_{SO}, respectively) during a meteorologically 'normal' period (±1 standard deviation from a long-term mean, see SI for more details). We compared data collected during periods when the wind farm was operational and idle at sites downwind and not downwind of wind turbines. Given the expected trend for stable boundary layers at night (warm air above cold air) and neutral (well-mixed) or unstable (cold air above warm air) boundary layers during the day, we also examined diurnal variation.

Materials and methods

Study area

This research was undertaken at Black Law Wind Farm, Scotland (55°46′01″N 03°44′20″W, elevation 250–320 m), which comprises 54 turbines within 18.6 km^2. The turbine blade hub heights are approximately 70 m, the rotor diameter 82 m and the total capacity is 124 MW. The wind farm was operational (hereafter referred to as ON) from 24th May 2012 to 7th June 2012, idle (hereafter OFF) from 12th June 2012 to 25th July 2012 and operational (ON) from 28th July to 15th November 2012. The switching on and off of the turbines was a phased operation lasting several days; data from this period were excluded from analysis. Given the commercial sensitivity of the data and the de-powering of the entire site, no wind data at hub height was available from which to calculate the capacity factor. However, the average capacity factor (i.e. the ratio of actual output compared to the maximum potential output) in the UK in 2012 was 26.2% (DECC 2014).

The vegetation across the wind farm comprised coniferous plantation (tree height up to approximately 20 m) and blanket bog, with a small amount of acid and improved grassland. However, most monitoring was undertaken in the blanket bog, with a limited number of sensors in grassland areas. The topography of the site was relatively flat, with most of the site lying between 260 and 320 m and with the topography varying predominantly in the north–south orientation (figure 1).

Data collection

Our field data collection framework was designed to capture the impacts on ecosystem processes within a wind farm, in terms of the scale, density and resolution, and did not undertake an energy balance approach. Air temperature (T_A) and relative humidity (RH) were measured every second and five-minute averages recorded at 2 m above the land surface (HOBO U23-002, Onset, USA; see SI). Sensors were deployed in a grid at 101 locations across a 2.6 by 1.4 km area of Black Law Wind Farm (figure 1). The elevation of the sampling locations varied from 277 to 305 m (no elevation corrections were required; see SI for details). Sensor resolution was 0.02 °C at 25 °C for temperature and 0.03% for RH. Surface and soil (−5 cm) temperatures (T_{SU} and T_{SO} respectively) were recorded every 30 min (HOBO Pendants, Onset, USA) at 36 locations, clustered at four sites (figure 1). Sensor resolution was 0.14 °C at 25 °C. At the same sites soil moisture (−10 cm) was measured every minute and averaged every 30 min (using a site-specific calibration) (CS625 water content reflectometers and CR200 loggers, Campbell Scientific Limited, UK). Sensor resolution was 0.1% volumetric water content. Wind direction was measured with a 2D sonic anemometer (Gill Instruments, UK) at site B, 2 m above the land surface every 10 s and averaged over 10 min intervals (figure 1). Wind speed resolution was 0.01 m s^{-1} and direction was 1°. All sensors were checked and calibrated prior to deployment. The sampling strategy was chosen to allow an adequate representation of the response of microclimate to wind turbine operation at a resolution appropriate for ecosystem processes (see SI). To ensure the period of field measurement was 'normal' we examined wind speed and stability and mixing ratios using data from nearby Met Office stations (see SI for full details).

Data processing

Sunrise and sunset are the meteorologically relevant temporal controls on boundary layer development (Stull 1998). Consequently, 'day' was classified as one hour after sunrise to one hour before sunset, as defined by the National Oceanic and Atmospheric Administration algorithm (ESRL 2014), and 'night' as one hour after sunset to one hour before sunrise (transition periods were excluded). As the Sun rose and set at significantly different times during the period of measurement, fraction of day was calculated, with sunrise as 0.0 (or 1.0), sunset as 0.5, and time linearly scaled between. The fraction of the day data were then categorised into 24 pseudo-hourly bins.

AH was derived from RH by first calculating the saturated water vapour pressure, then calculating the vapour pressure, and then finally the AH based upon temperature and vapour pressure (see SI for more information).

Departures were used in the analysis of the T_A, AH and RH data to remove diurnal and seasonal signals (the greatest controls) from the data. Essentially, the site-wide instantaneous mean was calculated for all measurement locations, and subtracted from each individual measurement, and then averaged over the ON and OFF periods and for downwind and not downwind groups where appropriate. In numerical form, the departures were derived by considering the vector of N temperature measurement locations at time t:

$$\underline{T}(t) = [T_1(t),\ T_2(t),\ \ldots,T_N(t)] \text{ for } t = t_1,\ t = t_2,\ldots,t = t_M \quad \text{(i. e. } M \text{ times in the sample set)} \tag{1}$$

then, calculating the site-wide scalar mean temperature at time $t = t_j$

$$T_{AV}(t_j) = \frac{1}{N}\sum_{i=1}^{N} T_i(t_j). \tag{2}$$

The vector of departures from the mean at time t_j

$$\underline{T}'(t_j) = [T_1(t_j) - T_{AV}(t_j),\ T_2(t_j) - T_{AV}(t_j),\ldots,\ T_N(t_j) - T_{AV}(t_j)] \tag{3}$$

allowing the time-averaged mean departure vector to be constructed:

$$\bar{\underline{T}}' = \left[\frac{1}{M}\sum_{j=1}^{M} T_1'(t_j),\ \frac{1}{M}\sum_{j=1}^{M} T_2'(t_j),\ \ldots,\ \frac{1}{M}\sum_{j=1}^{M} T_N'(t_j)\right]. \tag{4}$$

This vector is the one used in the paper, and when departures are mentioned they refer to this vector, or elements of it.

Variation in T_A, T_{SU}, T_{SO}, and AH was assessed by calculating the coefficient of variation (c_v) across the site for each measurement interval, and averaging in pseudo-hourly bins (based on fraction of the day) for ON and OFF periods (figure 3). Given the c_v of a population is defined as the standard deviation divided by the mean of the population ($c_v = \sigma/\mu$), the temperatures were first converted to degrees Kelvin to ensure meaningless values of c_v were not generated from negative or zero values of μ. The c_v was calculated using the same steps as above for T_A, AH and RH departures: the site-wide c_v was calculated and the time-averaged c_v vector constructed. In numerical form, at time $t = t_j$

$$c_v(t_j) = \frac{\frac{1}{N}\sum_{1}^{N}(T_i(t_j) - T_{AV}(t_j))^2}{T_{AV}(t_j)}, \tag{5}$$

where the temperature vector T and site-wide average T_{AV} are defined above (equations (1) and (2)). Analogous formulae apply to the other fields considered (AH and surface and soil temperatures). Note that the c_v was subsequently binned, according to time of

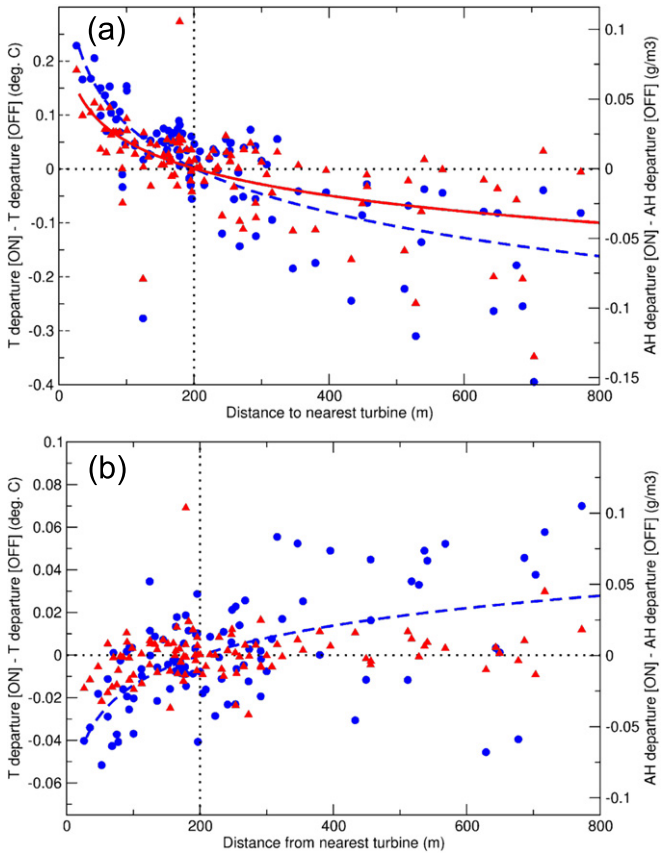

Figure 2. Turbine proximity influences observed effects of wind farm operation on T_A and AH. The effect of distance (x) from the nearest turbine on the temperature and AH departure during the night (a) and day (b). Blue dots represent the T_A departure difference for ON–OFF periods and red triangles the AH departure. The dotted blue lines and solid red lines represent the logarithmic approximation of the T_A and AH departures respectively. Black dotted lines represent the zero departure and 200 m distance baselines. To convert the x axis into multiples of rotor diameters, divide by 82 m.

day, giving a measure of spatial *and* temporal variability.

To examine the magnitude of effect of the turbines on T_A, RH and AH, only data when the wind direction at 2 m was from between 220° and 240° were considered. This directional sector was chosen as it was aligned with the main axis of the wind farm (figure 1), thus any cumulative effect of the turning turbines was likely to be greatest, and it was approximately the dominant wind direction. For the data to be included the wind had to be originating from between 220° and 240° at the measurement time *and* the previous 30 min, and also satisfy the day–night criteria for the entire 30 min period. This allowed the development of any underlying signal to be captured, while still providing a significant amount of data. Departures for all the data that fit these criteria were calculated for each sampling location, (see above), thus allowing the relative T_A, RH and AH of sites classified as downwind and not downwind of turbines to be compared. Further, as no hub height wind data was available, to take into account the potential effects of directional shear (between surface and hub height), we repeated the analysis for 200°–220°, 220°–240° and 280°–300° wind direction sectors. Unfortunately, given the layout of the wind farm, all measurement sites were classified as downwind in the 240°–260° and 260°–280° direction sectors. Given the complexity of wake dynamics, especially the interaction of multiple wakes, it was not appropriate to make assumptions regarding wake expansion and movement. Thus our analysis is prudent: measurement locations categorised as downwind (not downwind) may have been not downwind (downwind) of turbines and consequently the differences in T_A, RH and AH we quantified may be smaller than actual.

Statistics

Logarithmic best-fit lines were used to characterise the relationship between temperature and AH departure and distance to the nearest turbine (figure 2). Differences in c_v between ON and OFF periods for each pseudo-hour (figure 3) and temperature departures between downwind and not downwind groups were tested (table 1) using a paired t-test with unequal variances using Stata13 (StataCorp, Texas).

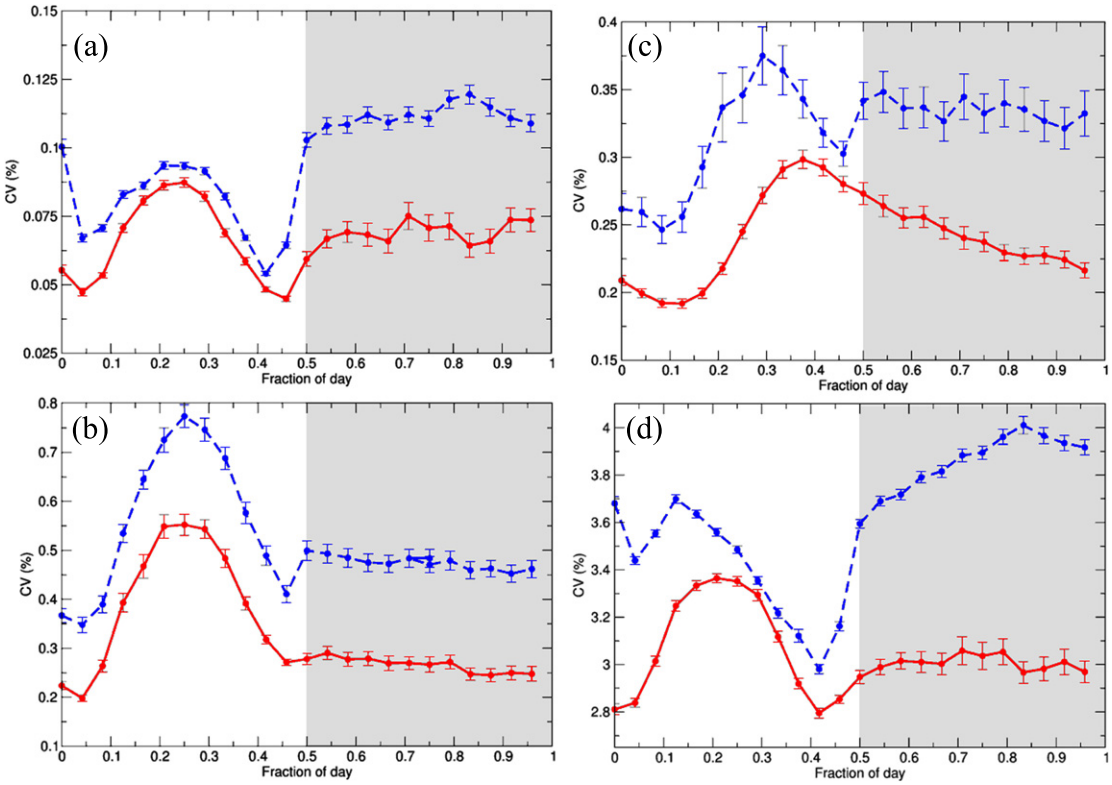

Figure 3. Diurnal variations in T_A, T_{SU} and T_{SO} and AH differ during wind farm operational and idle periods. Data points represent the average $c_v \pm$ standard error (SE) of the T_A (a), T_{SU} (b), T_{SO} (c) and AH (d) during the ON (blue dashed lines) and OFF (solid red lines) periods. Fraction of the day was calculated based on sunrise and sunset times (see methods), with 0 representing sunrise and 0.5 sunset and 0.04 approximately 1 h, with sunset to sunrise shaded grey.

Table 1. Temperature and absolute humidity differences between sites downwind and not downwind from turbines for three direction sectors during the night time. Differences are in °C for temperature and g m^{-3} for AH, positive values indicate the downwind locations were warmer and moister, negative values that downwind locations were cooler and drier, ns—not significant at $p < 0.05$.

Direction sector	T, ON, Night		T, OFF, Night		AH, ON, Night		AH, OFF, Night	
	p	Difference	p	Difference	p	Difference	p	Difference
200–220	<0.01	0.18	ns	0.04	<0.01	0.03	ns	0.00
220–240	<0.01	0.16	ns	−0.03	ns	0.00	ns	−0.03
280–300	ns	−0.06	ns	0.05	ns	0.03	ns	0.04

Results and discussion

Effects of wind turbine proximity on T_A and AH

To determine the integrated effect (i.e. irrespective of wind direction and speed) of the whole wind farm across the measurement period, we analysed the mean day and night-time differences in T_A and AH departure for each site from the site-wide mean between ON and OFF periods, using all data (i.e. data were not categorised as downwind or not downwind and therefore wake dynamics do not need to be considered). To assess the spatial extent of effects we related the departures to distance from the nearest turbine.

During the night, air closer to a wind turbine was warmer and more moist, with T_A departures reaching 0.25 °C and AH departures 0.1 g m^{-3} (figure 2(a)). Night-time warming and moistening has been attributed to downward mixing of warmer moister air by turbines during stable conditions (Baidya Roy 2011). The potential occurrence of this at Black Law is supported by analysis of midnight soundings from the two nearest upper-air stations: this reveals that during the most stable conditions the lapse rate is positive for both temperature and moisture (see SI) (Baidya Roy 2011). The larger effects closer to wind turbines could be the composite effect of that wind turbine and others upwind. This suggests that the interactions between multiple wakes may enhance effects found in single row turbine studies (Rajewski *et al* 2014). While positive departures are evident up to 200 m (2.4 rotor diameters) away (figure 2(a)), this does not suggest that effects of downward mixing were only evident within 200 m (2.4 rotor diameters) of a turbine. Compared to the site-wide mean, it was

generally warmer and more moist within 200 m (2.4 rotor diameters) of a turbine and cooler and drier beyond 200 m (2.4 rotor diameters). During the day, air closer to a wind turbine was cooler, with departures up to 0.05 °C, but AH was not influenced (figure 2(b)). This weaker day-time effect could be attributable to a convectively driven, well mixed boundary layer (Zhou *et al* 2013).

The trends between T_A departure ($\Delta T_A = T_A[ON] - T_A[OFF]$) during both day and night, and AH departure ($\Delta AH = AH[ON] - AH[OFF]$) at night, relative to distance from the nearest turbine (x), can be approximated by logarithmic functions: $\Delta T_A = 0.62 - 0.12 \ln(x)$, $r = 0.75$ and $\Delta AH = 0.15 - 0.03 \ln(x)$, $r = 0.61$ during the night and $\Delta T_A = -0.11 + 0.02 \ln(x)$, $r = 0.53$ during the day (figure 2). The daytime ΔAH cannot be approximated by a logarithmic function ($r < 0.2$). These logarithmic trends demonstrate that the effect of wind turbines can be quantified and thus potentially represented in models of Earth surface energy balance. This would be valuable given the complexity of extrapolating impacts from studies examining single or a single row of turbines (Rajewski *et al* 2014). Currently, model parametrisations (for example, Fitch *et al* (2012)) typically represent the effect of turbines on the atmosphere by imposing a sink of momentum and a source of turbulence kinetic energy. Multiple turbines are represented by integrating over a typical model grid cell (which may contain more than one turbine). With all such parametrisations a number of coefficients are required (such as the fraction of energy converted into turbulent kinetic energy—unknown *a priori*—which controls the subsequent mixing). Thus, the integrated effect we identified could be used to test such parameterisations of wind farms in numerical weather prediction models (Cervarich *et al* 2013), where the spatial resolution is greater than the distance between individual turbines, and the integrated effect of a whole wind farm needs to be established.

Diurnal effects of wind turbines on spatial variability in T_A, T_{SU}, T_{SO}, and AH

To quantify the spatio-temporal effects of wind turbine operation we examined the variation in T_A, T_{SU}, T_{SO}, and AH throughout the diurnal cycle (irrespective of wind direction and thus wake dynamics do not need to be considered). We used the coefficient of variation c_v of each of the measurements across the whole site for each measurement interval averaged for both the ON and OFF periods as a function of time of day. Using the c_v allows comparison of the ON and OFF periods: reporting this in degrees (such as would be obtained by the standard deviation) would be misleading as the temperature is more variable in summer months compared with autumn months.

The spatial variations in the T_A, T_{SU}, T_{SO} and AH data were significantly greater during the ON period compared with the OFF period ($p < 0.05$ for pseudo 10:00 and 11:00 for the T_{SO} data and pseudo 07:00 for the AH data, $p < 0.01$ for all other data and hour intervals) (figure 3), suggesting turbine operation increased vertical mixing and turbulence. This effect, at several levels (i.e. soil, surface, and air at 2 m), has not been identified in other field studies but has been reported in modelling studies (Lu and Porté-Agel 2015). The spatial variance in microclimate is of crucial importance as ecosystem processes respond to small-scale variation in climate (Baidya Roy *et al* 2004, Baidya Roy and Traiteur 2010, Baidya Roy 2011, Zhou *et al* 2012, De Frenne *et al* 2013, Rajewski *et al* 2013, Smith *et al* 2013, Zhou *et al* 2013). The differences in temperature variation between ON and OFF periods were greatest for T_{SU} data (figure 3(b)) and smallest for T_A data (figure 3(a)), reflecting relatively well-mixed air at 2 m and increased variability at the surface arising from peatland micro-topography and vegetation shading. AH aside, the spatial variance was greatest for T_{SU} and least for T_A, during ON and OFF periods (figure 3). This is attributable to the patchy influence of vegetation shading and surface water content on the temperatures of the surface sensors. Further, peatland temperatures are highly spatially variable, in response to the peat thermal properties (Kettridge and Baird 2010), thus explaining the T_{SO} spatial variability. In contrast, although there are differences across the wind farm, the air max is relatively well mixed.

The difference in T_A and AH variability between the ON and OFF periods was greater during night than day (figures 3(a) and (d)), whereas it was approximately equal for T_{SU} and T_{SO}, with smaller differences during transition periods around sunrise and sunset (figures 3(b) and (c)). This suggests that night-time T_A and AH were most sensitive to turbines, due to downward mixing of warm air. Further, the mixing down of warm air during the ON period appears to have affected the diurnal trend in T_{SO} and AH: the maximum variability in T_{SO} and AH were later in the day during the OFF period compared with the ON period (figures 3(c) and (d)). This suggests that the night-time background gradient of T_{SO} and AH are eroded by turbulence earlier in the day during the ON period. No trends in soil moisture were found (see SI) probably as a result of the high water table across the wind farm (Armstrong *et al* 2015).

Downwind effects of wind turbines on T_A and AH

Our final analysis examined the magnitude of effect of wind turbines on T_A and AH during the night (see SI for day-time and RH results) when we observed a strong relationship between T_A and AH departures and distance from the turbine (figure 2). Consequently, we excluded all data from one hour before sunrise to one hour after sunset and filtered for wind

directions between 220° and 240° (aligned along the main axis of the wind farm) (figure 1). Temperature departures for all the data that fit these criteria were calculated for each sampling location, thus allowing the relative T_A and AH of sites downwind and not downwind of turbines to be compared. Directional shear between hub height and the surface, both clockwise and anticlockwise, can occur (Walter *et al* 2009, Cariou *et al* 2010, Rhodes and Lundquist 2013), and consequently we also analysed the data filtered for wind directions between 200°–220°, 220°–240° and 280°–300°.

We found that temperatures were significantly warmer in areas downwind of turbines during the ON period ($p < 0.01$), with an average relative warming of 0.18 °C for the 200°–220° direction sector and 0.16 °C for the 220°–240° sector (table 1). The AH of air downwind of the turbines was, on average, 0.03 g m^{-3} greater during the ON period ($p < 0.01$) for the 200°–220° direction sector but there was no significant difference for the 220°–240° sector (table 1). This suggests that there may have been slight anti-clockwise directional shear in the boundary layer, although we cannot rule out stronger slightly clockwise shear as all sites were downwind of turbines in the 240°–260° and 260°–280° sectors. Although clockwise shear is expected given the Ekman spiral, anti-clockwise shear has been observed previously (Walter *et al* 2009) and could have been caused by the wind turbines disturbing the atmospheric boundary layer.

Analysis of the data shows that the relative increase in saturated water vapour pressure had more effect on AH than the combined increase in temperature, and lowering of RH (see SI), consistent with turbine-induced mixing of warmer and more moist air downwards (Baidya Roy *et al* 2004). During the OFF period, temperature and AH departures were variable with no statistically significant difference between downwind and not downwind sites ($p > 0.05$), further demonstrating the variation during the ON period was due to wind turbine operation (table 1).

The impacts of temperature change on ecosystem carbon cycling

Terrestrial carbon cycling is highly variable, both spatially and temporally, and influenced by many biotic and abiotic conditions and their interactions, as demonstrated at this site (Armstrong *et al* 2015). Given this, and the relatively small variation in microclimate between ON and OFF periods compared to spatial and temporal variability, it was not possible to measure the impact of wind farm operation on carbon cycling. However, peatlands are highly temperature sensitive environments, and consequently these observed small-scale changes in temperature could have significant implications for peatland carbon stocks. For example, during the growing season, a 0.88 °C warming was found to increase rates of ecosystem respiration in a peatland in northern England by 20% and decrease net CO_2 uptake by 11% (Ward *et al* 2013). In contrast, during the non-growing season when CO_2 fluxes were much lower, a 0.72 °C warming increased ecosystem respiration rates by 44% and CO_2 uptake by 7% (Ward *et al* 2013). Therefore, as we found night time warming was most influenced, decomposition processes may be accelerated and thus soil carbon losses observed. However, effects on respiration could also be offset by plant physiological responses to warming (Peng *et al* 2013). Our results also indicated that wind farm operation had greater effects on spatial and diurnal variability in T_{SU} and T_{SO} than T_A. T_{SU} and T_{SO} are recognised as stronger regulators of plant-soil carbon dynamics (Graae *et al* 2012, De Frenne *et al* 2013); consequently, the effects on the net carbon balance of the hosting ecosystem may be stronger than inferred from T_A (Baidya Roy and Traiteur 2010, Rajewski *et al* 2013, Smith *et al* 2013).

Conclusion

This research provides the first field evidence that operational wind turbines can have a measureable effect on soil and soil surface temperature, and demonstrates the effect of multiple turbine wakes on air temperature and humidity. When the turbines were operational we found greater variability in temperature (soil, soil surface and air) and AH throughout the diurnal cycle with T_A and AH increasing at night. Whilst the effects were statistically significant, the observed differences were small compared with spatial variation recorded across the site. Importantly, we also demonstrate that the effects on both T_A and AH can be described by a logarithmic function of distance from nearest turbine, a generic approach showing for the first time how the *integrated effect* of a wind farm may be estimated.

This research demonstrates that effects of wind turbines on ground-level microclimate could have implications for biogeochemical processes and ecosystem carbon cycling. Consequently, improved measurements and modelling approaches are needed to determine the true carbon balance of wind energy that includes the effects of altered ground-level microclimates.

Acknowledgments

This research was supported by the UK Natural Environment Research Council (NE/H01036X/1, NE/H010351/1, NE/H010335/1). AA acknowledges financial support from an Energy Lancaster fellowship during which she undertook data analysis and manuscript preparation. We thank Scottish Power Renewables and the land owners for allowing site access. We thank Martin Coleman, Ross Herbert, Hemanth

Pasumarthi, Salvatore Peppe, Harriet Richardson, Kenny Roberts, Fraser Russell, Gavin Thompson, Bethan White and Scott Wylie for assistance in the field, and Barbara Brooks, James Groves, Salvatore Peppe and Felicity Perry for assistance calibrating the loggers.

The authors would like to thank the anonymous reviewers whose comments and suggestions have greatly improved this paper.

References

Armstrong A, Waldron S, Ostle N J, Richardson H and Whitaker J 2015 Biotic and abiotic factors interact to regulate northern peatland carbon cycling *Ecosystems* **18** 1395–409

Armstrong A, Waldron S, Whitaker J and Ostle N J 2014 Wind farm and solar park effects on plant-soil carbon cycling: uncertain impacts of changes in ground-level microclimate *Glob. Change Biol.* **20** 1699–706

Baidya Roy S 2011 Simulating impacts of wind farms on local hydrometeorology *J. Wind Eng. Ind. Aerodyn.* **99** 491–8

Baidya Roy S, Pacala S W and Walko R L 2004 Can large wind farms affect local meteorology? *J. Geophys. Res.* **109** D19101

Baidya Roy S and Traiteur J J 2010 Impacts of wind farms on surface air temperatures *Proc. Natl Acad. Sci.* **107** 15679–84

Cariou N, Wagner R and Gottschall J 2010 Analysis of vertical wind direction and speed gradients for data from the met. mast at Høvsøre. Roskilde: Danmarks Tekniske Universitet, Risø Nationallaboratoriet for Bæredygtig Energi (Denmark. Forskningscenter Risoe. Risoe-R; No. 1733(EN)) (http://orbit.dtu.dk/files/4548949/ris-r-1733.pdf)

Cervarich M C, Roy S B and Zhou L 2013 Spatiotemporal structure of wind farm-atmospheric boundary layer interactions *Energy Procedia* **40** 530–6

De Frenne P *et al* 2013 Microclimate moderates plant responses to macroclimate warming *Proc. Natl Acad. Sci. USA* **110** 18561–5

DECC 2014 Load factors for renewable electricity generation (DUKES 6.5) *Digest of United Kingdom Energy Statistics, Renewable Sources of Energy* ch 6 (London, UK: Department of Energy and Climate Change) (www.gov.uk/government/uploads/system/uploads/attachment_data/file/279523/DUKES_2013_published_version.pdf)

Denholm P, Hand M, Jackson M and Ong S 2009 Land-use requirements of modern wind power plants in the united states *National Renewable Energy Laboratory* (Colorado: US Department of Energy) (www.nrel.gov/docs/fy09osti/45834.pdf)

ESRL 2014 *Solar Calculation Details*, Earth System Research Laboratory (http://esrl.noaa.gov/gmd/grad/solcalc/calcdetails.html) (accessed 3 April 2015)

Fiedler B H and Bukovsky M S 2011 The effect of a giant wind farm on precipitation in a regional climate model *Environ. Res. Lett.* **6** 045101

Fitch A C, Olson J B, Lundquist J K, Dudhia J, Gupta A K, Michalakes J and Barstad I 2012 Local and mesoscale impacts of wind farms as parameterized in a mesoscale NWP model *Mon. Weather Rev.* **140** 3017–38

Graae B J *et al* 2012 On the use of weather data in ecological studies along altitudinal and latitudinal gradients *Oikos* **121** 3–19

GWEC 2015 *Global Wind Statistics 2014* (Brussels, Belgium: Global Wind Energy Council) (www.gwec.net/wp-content/uploads/2015/02/GWEC_GlobalWindStats2014_FINAL_10.2.2015.pdf)

IEA 2012 *World Energy Outlook 2012: Renewable Energy Outlook* (Paris, France: International Energy Association) (www.worldenergyoutlook.org/media/weowebsite/2012/weo2012_renewables.pdf)

Keith D W, Decarolis J F, Denjenberger D C, Lenschow D H, Malyshev S L, Pacala S and Rasch P J 2004 The influence of large-scale wind power on global climate *Proc. Natl Acad. Sci. USA* **101** 16115–20

Kettridge N and Baird A J 2010 Simulating the thermal behavior of northern peatlands with a 3D microtopography *J. Geophys. Res.* **115** G03009

Knopper L and Ollson C 2011 Health effects and wind turbines: a review of the literature *Environ. Health* **10** 78

Lovich J E and Ennen J R 2013 Assessing the state of knowledge of utility-scale wind energy development and operation on non-volant terrestrial and marine wildlife *Appl. Energy* **103** 52–60

Lu H and Porté-Agel F 2015 On the impact of wind farms on a convective atmospheric boundary layer *Bound.-Layer Meteorol.* **157** 81–96

Northrup J M and Wittemyer G 2013 Characterising the impacts of emerging energy development on wildlife, with an eye towards mitigation *Ecol. Lett.* **16** 112–25

Pearce-Higgins J W, Stephen L, Douse A and Langston R H W 2012 Greater impacts of wind farms on bird populations during construction than subsequent operation: results of a multi-site and multi-species analysis *J. Appl. Ecol.* **49** 386–94

Peng S *et al* 2013 Asymmetric effects of daytime and night-time warming on Northern Hemisphere vegetation *Nature* **501** 88–92

Rajewski D A *et al* 2013 CWEX: Crop/Wind-energy experiment: observations of surface-layer, boundary-layer and mesoscale interactions with a wind farm *Bull. Am. Meteorol. Soc.* **94** 655–72

Rajewski D A, Takle E S, Lundquist J K, Prueger J H, Pfeiffer R L, Hatfield J L, Spoth K K and Doorenbos R K 2014 Changes in fluxes of heat, H_2O, and CO_2 caused by a large wind farm *Agric. Forest Meteorol.* **194** 175–87

Rhodes M and Lundquist J 2013 The effect of wind-turbine wakes on summertime US midwest atmospheric wind profiles as observed with ground-based doppler lidar *Bound.-Layer Meteorol.* **149** 85–103

Smith C M, Barthelmie R J and Pryor S C 2013 In situ observations of the influence of a large onshore wind farm on near-surface temperature, turbulence intensity and wind speed profiles *Environ. Res. Lett.* **8** 034006

Stull R B 1988 *An Introduction to Boundary Layer Meterology* (Dordrecht: Kluwer)

Walter K, Weiss C C, Swift A H, Chapman J and Kelley N D 2009 Speed and direction shear in the stable nocturnal boundary layer *J. Sol. Energy Eng.* **131** 011013

Wang C and Prinn R G 2010 Potential climatic impacts and reliability of very large-scale wind farms *Atmos. Chem. Phys.* **10** 2053–61

Ward S E, Ostle N J, Oakley S, Quirk H, Henrys P A and Bardgett R D 2013 Warming effects on greenhouse gas fluxes in peatlands are modulated by vegetation composition *Ecol. Lett.* **16** 1285–93

Zhou L, Tian Y, Baidya Roy S, Dai Y and Chen H 2013 Diurnal and seasonal variations of wind farm impacts on land surface temperature over western Texas *Clim. Dyn.* **41** 307–26

Zhou L, Tian Y, Baidya Roy S, Thorncroft C, Bosart L F and Hu Y 2012 Impacts of wind farms on land surface temperature *Nat. Clim. Change* **2** 539–43